ACS Photonics

Article

pubs.acs.org/journal/apchd5

Current–Voltage Enhancement of a Single Coaxial Nanowire Solar Cell

Sunil Sandhu and Shanhui Fan*

Department of Electrical Engineering, Stanford University, Stanford, California 94305, United States

ABSTRACT: We show that the absorption cross-section of a single absorbing nanowire can be significantly enhanced over a broad bandwidth by coating the nanowire with a transparent dielectric to create a coaxial nanowire. The coating, while by itself is not absorbing, increases the number of resonances supported by the wire and also enhances the coupling to incident light, resulting in the enhancement of absorption cross-section. When operating as a solar cell, we show that the short-circuit current of a GaAs nanowire coated with Al_2O_3 is strongly enhanced over that of the bare GaAs nanowire with the same absorbing volume. This addition of the transparent dielectric layer maintains the open-circuit voltage enhancement of the bare nanowire over that of a bulk GaAs cell. Similar large current–voltage enhancements are also presented for a Si nanowire coated with SiO_2.

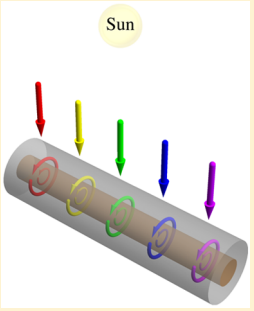

KEYWORDS: *coaxial nanowire, absorption cross-section, angular momentum channel, Mie resonance, solar cell, detailed balance*

When designing nanostructured solar cells, it is important to reduce the active volume of the cell without any penalty to its absorption.[1−4] Consequently, there has been considerable recent interest in developing solar cells consisting of single semiconductor nanowires, since the absorption cross-section of a nanowire can significantly exceed its geometric cross-section.[5−15] A properly designed single nanowire can deliver a much higher current in comparison to an equal-volume bulk cell with the same amount of material.[16] Moreover, the strong confinement of light by the single nanowire can also result in an open-circuit voltage that is higher than that of the bulk cell.[15,16] There have also been recent works that showed that the absorption cross-section of a single nanowire can be further enhanced while keeping its absorption volume fixed. Ways to do this include (a) inserting a metal core into the absorbing nanowire[17,18] and (b) coating the absorbing nanowire with an effective antireflection layer of appropriate thickness.[19,20]

In this letter, we show that a *coaxial* nanowire, in which a transparent dielectric layer is coated around an absorbing nanowire, can have a significantly larger absorption cross-section over a broad bandwidth when compared to a corresponding bare nanowire without the transparent layer. We demonstrate that the absorption enhancement comes from enhanced coupling to incident light in addition to an increased number of resonances supported by the nanowire. Moreover, the use of such a transparent layer also preserves the voltage enhancement capability of the bare nanowire. An illustration of our results is presented in Figure 1, which compares the current–voltage characteristics between an optimized GaAs bare nanowire and the same bare nanowire coated with a ΔR = 100 nm thick Al_2O_3 layer, i.e., a coaxial wire. We can see from Figure 1b that a considerably larger short-circuit current enhancement of ∼60% results from just coating the absorbing bare nanowire with this transparent oxide layer. In addition, the coaxial wire has an open-circuit voltage that is similar to that of the bare wire[16] and that is signifiantly higher than that of a bulk GaAs cell.[21]

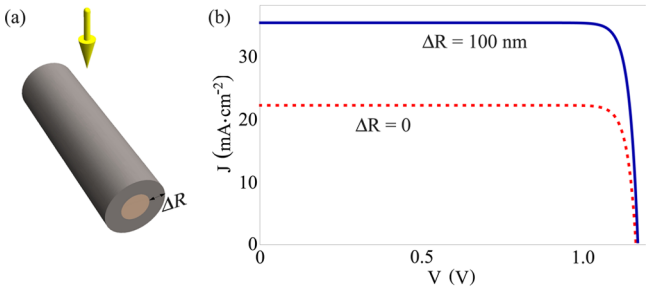

Figure 1. (a) Schematic of a coaxial nanowire with an outer layer transparent dielectric coating of thickness ΔR. The center region consists of the absorbing nanowire, while the outer region consists of a transparent dielectric. Yellow arrow indicates the direction of incident sunlight. (b) Current density–voltage (J–V) characteristics of a coaxial GaAs nanowire with and without a ΔR = 100 nm thick Al_2O_3 coating. For both plots in (b), the radius of the absorbing GaAs wire region is r = 73 nm.

In what follows, we will start by giving a qualitative overview of the optical physics that control the absorption cross-section spectrum of a single nanowire. We specifically study the two main factors that influence this absorption spectrum of the wire: (i) the wire's interaction with an external incident wave and (ii) the number of resonances it supports. On the basis of these considerations, we then explain the large absorption enhancement in coaxial nanowires, using the example of a GaAs wire with an outer layer Al_2O_3 coating. We next show that such absorption enhancement can coexist with voltage enhancement

Received: May 1, 2015
Published: November 12, 2015

DOI: 10.1021/acsphotonics.5b00236
ACS Photonics 2015, 2, 1698–1704

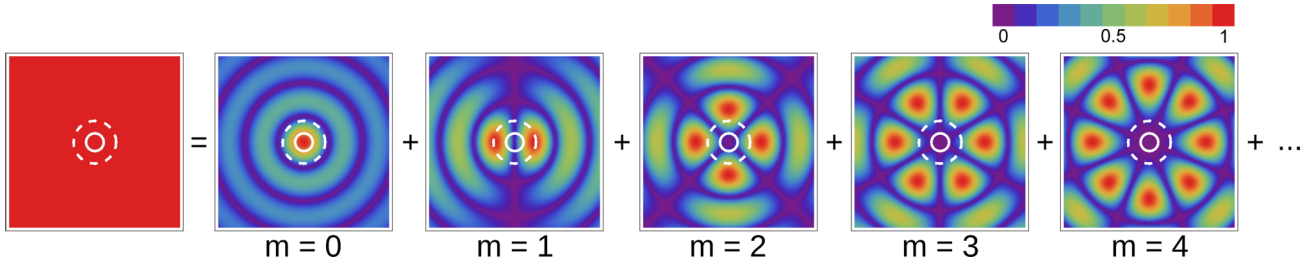

Figure 2. Expansion of a normally incident TM plane wave $E^{\text{incident,TM}}$ with wavelength λ_0 = 550 nm and magnitude E_0 = 1 into a sum of cylindrical waves (eq 1). Field plot of the incident electric field magnitude profile $|E^{\text{incident,TM}}|$ is shown on the left-hand side, and field plot of the electric field magnitude profile $|E_m^{\text{incident,TM}}|$ associated with each of the first five angular momentum channels m is shown on the right-hand side. The inner solid white circle in all plots represents the circumference of a r = 73 nm radius absorbing nanowire, while the outer dashed white circle represents the circumference of a ΔR = 100 nm thick transparent coating layer (Figure 1). The electric field magnitude values in each field plot are represented by the color scale in the top right corner.

in nanowire structures. Finally, we present the current−voltage characteristics of a coaxial Si wire with an outer layer SiO_2 coating, which demonstrates similar absorption enhancement to the GaAs-Al_2O_3 coaxial structure.

A nanowire solar cell absorbs sunlight incident from free space. Therefore, its absorption properties need to be understood in terms of both (i) the properties of light in free space, as characterized by angular momentum channels, and (ii) the properties of the wire itself, as characterized by the resonance modes within the wire.[22−24] To illustrate the properties of light in free space, we consider the scenario of a transverse magnetic (TM) plane wave that is normally incident on the wire as shown in Figure 1a. For a TM wave, the electric field is polarized parallel to the nanowire's longitudinal axis. Such an incident plane wave can be expanded in terms of the basis of cylindrical wave channels, each associated with a unique angular momentum number m:[5,25]

$$E^{\text{incident,TM}} = E_0 e^{ik_0 x} = \sum_{m=0}^{\infty} E_m^{\text{incident,TM}}$$

$$E_m^{\text{incident,TM}} = E_0 J_m(k_0 r) e^{im\pi/2} \cos(m\phi)(2 - \delta_m) \quad (1)$$

In eq 1, E_0 is the amplitude of the incident plane wave, $k_0 = \frac{2\pi}{\lambda_0}$ is its wave vector, λ_0 is its free space wavelength, and x is the spatial coordinate in the direction of propagation (yellow arrow in Figure 1a). $E_m^{\text{incident,TM}}$ is the component of $E^{\text{incident,TM}}$ in the mth angular momentum channel, $J_m(kr)$ is the mth order Bessel function of the first kind, and δ_m is the Kronecker delta function. ϕ and r are the azimuthal angle and radial position, respectively, in cylindrical coordinates. The $\cos(m\phi)$ factor arises because the incident plane wave is even with respect to the plane that includes both the incident wave's propagation direction and the wire's longitudinal axis.

To understand how the different channels of the incident wave interact with a bare nanowire, Figure 2 shows the incident electric field magnitude profile $|E^{\text{incident,TM}}|$ in addition to the profiles for the first few channel components $|E_m^{\text{incident,TM}}|$, overlaid on the bare nanowire cross-section (region within solid white inner circle). In Figure 2, the wavelength of the incident wave is λ_0 = 550 nm, while the radius of the bare wire is r = 73 nm. We notice from the figure that except for the m = 0 angular momentum channel, in all other channels the components of the incident field have zero magnitude at the wire center r = 0. Moreover, as m increases, there is an increased suppression of the electric field within the wire.

This observed behavior of the incident wave's electric field components in Figure 2 is expected based on the characteristics of the Bessel function $J_m(k_0 r)$ associated with channel m in eq 1. Particularly, $J_m(k_0 r)$, which controls the radial distribution of the mth channel electric field, asymptotically varies[26] as $\frac{1}{m!}\left(\frac{k_0 r}{2}\right)^m$ when $k_0 r \ll \sqrt{m+1}$, i.e., close to the wire center r = 0. Therefore, the electric field associated with channel m is increasingly suppressed within the wire as m increases. For example, in the case of the r = 73 nm bare wire in Figure 2, we see that there is a significantly reduced overlap of the wire with angular momentum channels m = 2 onward. Consequently, these higher angular momentum channels are weakly coupled to the nanowire.[23,24]

Having considered the properties of free space in terms of angular momentum channels, we next consider the properties of the resonance modes within the wire. Each resonance here is associated with a cylindrical wave in the wire with a unique angular momentum as numbered by m, and for a wire of a given radius r, there is an upper limit to the maximum angular momentum of the resonances that can be supported within the wire. We can illustrate this upper limit by first expanding the wire's internal electric field in terms of the basis of cylindrical waves (assuming the wire is excited by the normally incident TM wave in eq 1):[5,25]

$$E^{\text{internal,TM}} = \sum_{m=0}^{\infty} E_m^{\text{internal,TM}}$$

$$E_m^{\text{internal,TM}} = a_m J_m(kr) \cos(m\phi)(2 - \delta_m) \quad (2)$$

In eq 2, $E_m^{\text{internal,TM}}$ is the electric field of the cylindrical wave component whose angular momentum is numbered by m and whose amplitude is a_m. Similar to the case of the incident wave in eq 1, the radial distribution of $E_m^{\text{internal,TM}}$ is represented by $J_m(kr)$. However, unlike eq 1, here the argument of the Bessel function involves a wavevector within the wire $k = nk_0$ with n being the complex refractive index of the wire at the free space wavelength λ_0. Therefore, in contrast to cylindrical waves in air, the larger wave vector $k = nk_0$ within the wire results in the peaks of all the cylindrical waves in eq 2 being closer to the center of the nanowire.

As m increases in eq 2, the corresponding radial field is asymptotically *pushed out* of the wire. Therefore, the wire will not support a resonance with high angular momentum. Specifically, the wire can only support a resonance with an

DOI: 10.1021/acsphotonics.5b00236
ACS Photonics 2015, 2, 1698−1704

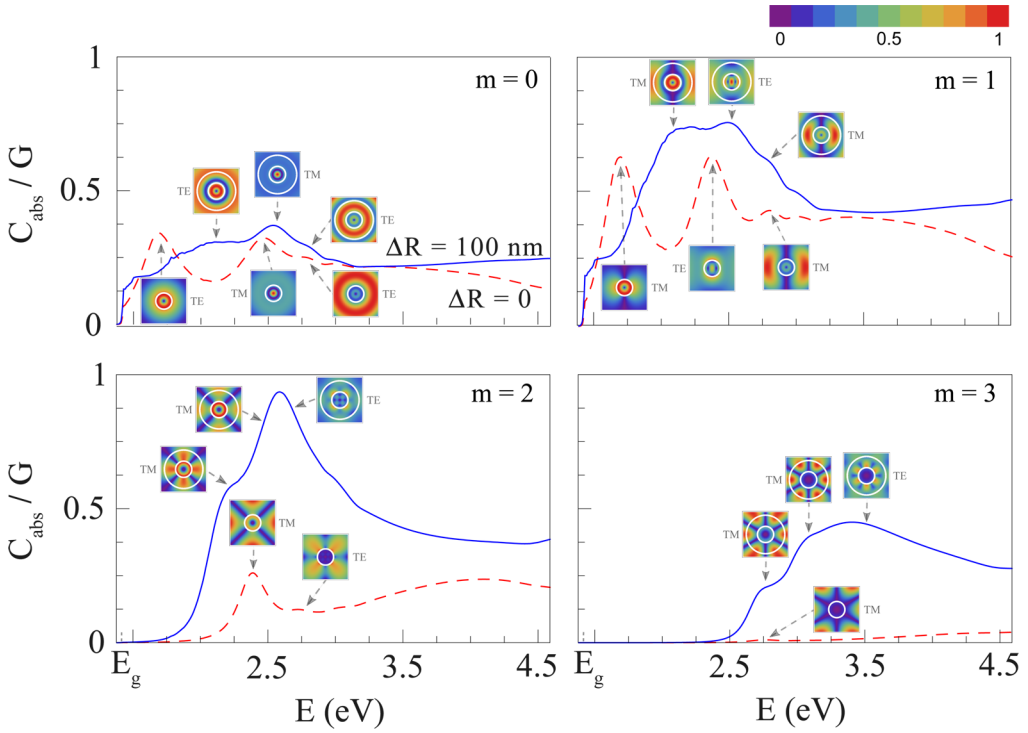

Figure 3. Normal incidence absorption efficiency spectra for the first four angular momentum channels (m = 0 to 3) of a radius r = 73 nm GaAs nanowire with (solid blue line) and without (dashed red line) a ΔR = 100 nm thick outer layer Al_2O_3 coating. All spectra are shown starting from E = 1.38 eV, and the GaAs direct band gap is located at E_g = 1.42 eV. Also shown within each plot are the electric field magnitude profiles for some of the prominent TE and TM resonances of both the bare and coaxial wires. The field profiles above (below) the blue solid line in each plot are those for the coaxial (bare) wire case. The two solid white circles in the coaxial wire field profiles represent the circumferences of the coaxial layers, while the solid white circle in the bare wire field profiles represent the circumference of the bare wire. The electric field magnitude values in each field profile have been scaled to lie between 0 and 1, as represented by the color scale in the top right corner.

angular momentum that has a number m, which satisfies the following whispering gallery condition:[23,24]

$$2\pi m \leq \beta 2\pi r \tag{3}$$

In eq 3, β is the wave vector $k = nk_0$ in the case of the bare nanowire.

In studying the characteristics of the incident and internal electric fields above, we have specialized to the case of a TM-polarized incident plane wave. However, we note that the case of an orthogonally polarized incident plane wave, i.e., transverse electric (TE) polarized wave, has similar characteristics in both its incident fields in free space and its internal fields within the wire.[5,25] Therefore, the discussions apply to both TM and TE waves.

Hence, in the nanowire's interaction with light its radius plays the following two roles: (i) it limits the number of channels of the incident light that the wire can couple into, and (ii) it limits the number of resonances that the wire can support. Accordingly, we reach the following conclusions regarding the nanowire's radius. First, one way to strongly couple to the higher angular momentum channels of an external incident wave is to increase the radius of the nanowire. We emphasize here that it is the wire's physical radius and not its absorber radius that matters. Therefore, coating an absorbing bare nanowire with a transparent layer will increase the coupling to these higher angular momentum channels (as depicted by the outer dashed white circle in each field plot of Figure 2). The increased physical area from the coating results in a better overlap with the fields of the higher angular momentum channels.

Second, the increase in physical radius from a transparent outer layer also allows the wire to support resonances with higher angular momentums (that are otherwise inaccessible to the smaller radius bare nanowire). Therefore, adding a transparent layer also helps to increase the number of resonances within the wire. Consequently, the absorption of incident light by such a coaxial nanowire will be significantly enhanced beyond that of a bare nanowire with the same absorbing volume.

As an illustration of the physical principle discussed above, Figure 3 compares the absorption efficiency spectra associated with the first four angular momentum channels of light normally incident on a r = 73 nm GaAs bare nanowire with and without a ΔR = 100 nm thick Al_2O_3 coating. The r = 73 nm bare nanowire was optimized for current−voltage performance in ref 16. The material parameters required for calculating the absorption spectra in Figure 3 were extracted from refs 27 and 28. Also included within each of these absorption plots are the electric field magnitude profiles of some of the prominent TM and TE resonances for both the bare and coaxial wire cases (for example, $|E_m^{\text{internal,TM}}|$ in eq 2 in the case of the TM resonances).

The absorption efficiency in this article is defined as the ratio of the absorption cross-section C_{abs} to the absorbing volumes's geometrical cross-sectional area G.[5,16] For example, in the case of a length l section of a coaxial wire with GaAs radius r shown in Figure 1:

$$G = 2r \times l \tag{4}$$

DOI: 10.1021/acsphotonics.5b00236
ACS Photonics 2015, 2, 1698−1704

For all absorption efficiency plots in this article, we show the average absorption efficiency of both the TM and TE polarizations.

Considering the bare nanowire case first, we see from Figure 3 that whereas it has strong absorption efficiency for the first two angular momentum channels m = 0 and 1, its absorption efficiency is weaker for the m = 2 channel and, furthermore, negligible for the m = 3 channel. This is an expected result based on our discussion on the properties of light in free space and within the wire. Specifically, Figure 2 shows that there is little overlap of the r = 73 nm bare wire (solid white line) with channels m = 2 and 3 of the incoming light at wavelength λ_0 = 550 nm, for example. Moreover, a calculation from eq 3 gives a value of m = 3 for the upper limit associated with the angular momentum of any resonance that can be supported by the r = 73 nm bare wire at λ_0 = 550 nm. For example, in Figure 3 we see prominent resonant behaviors only with m = 0, 1, and 2 in the bare wire case.

On the other hand, for the nanowire with an Al_2O_3 coating, we see that the absorption efficiency spectra of the higher angular momentum channels (m = 2 and 3) in Figure 3 are strongly enhanced over those of the bare nanowire. Furthermore, the absorption of the lower angular momentum channels is also significantly enhanced over that of the bare wire for a large part of the displayed spectrum. The significant absorption efficiency increase of the coaxial wire is partly due to increased overlap of its physical cross-section with the higher channels of incoming light. This is shown in Figure 2, where the outer dashed circle depicts the coaxial wire. In addition, eq 3 indicates that the larger physical radius of the coaxial wire allows it to support resonances with a higher angular momentum as compared to that of a bare wire, as seen in the panel in Figure 3 that corresponds to m = 3.

The total absorption efficiency, defined as the sum of the absorption efficiency over all angular momentum channels, is shown in Figure 4 for the case of normally incident light. The strongly enhanced absorption of the coaxial wire over that of the bare wire is immediately apparent from this plot. The enhancement occurs for most of the photon energies above the GaAs band gap. This is a remarkable result considering that we have an equal amount of absorbing material volume in both the bare wire and coaxial wire cases, and although we considered only normally incident light in Figure 4, the same absorption enhancement in the coaxial wire case occurs for a wide range of incident angles.

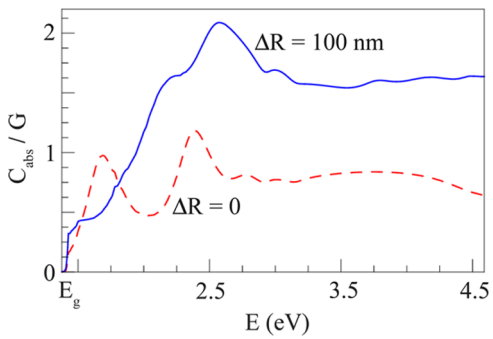

Figure 4. Normal incidence total absorption efficiency spectra of a radius r = 73 nm GaAs nanowire with (solid blue line) and without (dashed red line) a ΔR = 100 nm thick outer layer Al_2O_3 coating. Both spectra are shown starting from E = 1.38 eV, and the GaAs direct band gap is located at E_g = 1. 42 eV.

Up to now, we have calculated the absorption efficiency spectra of the GaAs-Al_2O_3 coaxial nanowire solar cell. Using a detailed balance analysis, we will next translate this absorption spectra into a current density−voltage (J−V) characterization of the coaxial cell.[16,29] The absorption efficiency spectra controls both the nanowire's absorption and emission properties that enter into this detailed balance analysis. A detailed documentation of this detailed balance analysis for a nanowire can be found in ref 16.

Our J−V characterization of the GaAs-Al_2O_3 coaxial cell will involve calculating its short-circuit current density J_{sc}, open-circuit voltage V_{oc}, and efficiency at the maximum power point.[16,29] For the J_{sc}, we need only the cell's radiative generation rate F_g, which can be calculated from the absorption efficiency spectra at normal incidence in Figure 4 (see eq 2 in ref 16).

On the other hand, in order to determine the cell's V_{oc}, the detailed balance analysis requires the evaluation of the cell's thermal equilibrium radiative recombination rate F_{co}, which can be determined from the cell's absorption efficiency spectra over all angles of incidence.[16,29]

From the J_{sc} and V_{oc} values of the coaxial cell, its efficiency at the maximum power point can be calculated as $\mathrm{FF}\frac{J_{sc}V_{oc}}{P_{inc}} \times 100\%$. Here P_{inc} is the total incident sun radiation power per unit cell area, and FF is the cell's fill-factor.[29] We note that the efficiency of a single nanowire cell can be large due to its funneling of incident sunlight, i.e., its large absorption cross-section.[5]

In all J−V characterizations in this article, we consider only the ideal case of a defect-free coaxial nanowire with perfect surface passivation, in order to establish a better understanding of how optical physics influences the nanowire's J−V performance. The analysis considers only intrinsic recombination mechanisms, which includes radiative and Auger recombinations.[21] In the case of the Auger recombination mechanisms in GaAs, following ref 21 we assume the cell is approximately intrinsic under illumination.[30,31]

Furthermore, even though we do include the fundamental Auger nonradiative recombination rate in all our V_{oc} calculations below, we note that for the GaAs-based coaxial nanowire solar cells considered in this letter, the radiative rate dominates over this Auger nonradiative rate. This allows us to approximate the cell's V_{oc} as follows:[32]

$$V_{oc} \approx \frac{k_B T_c}{q} \log\left(\frac{F_g}{F_{co}}\right) \tag{5}$$

In eq 5, k_B is the Boltzmann constant, T_c is the ambient temperature, and q is the electron charge. Therefore, we see that for the GaAs-Al_2O_3 coaxial wires the V_{oc} is strongly influenced by the contrast ratio between F_g and F_{co}.

The blue solid lines in Figure 5 plot the J−V characteristics for a GaAs-Al_2O_3 coaxial wire as a function of Al_2O_3 thickness ΔR (with the radius of the inner absorbing GaAs section fixed at r = 73 nm), while the red dotted lines plot the J−V characteristics for a bare GaAs nanowire with the same total radius 73 nm + ΔR as the coaxial wire. In comparing the coaxial wire to the bare wire here, we normalize J and, thus, the efficiency of the nanowires to the geometric cross-section area of the absorber section. Such a normalization makes sense

DOI: 10.1021/acsphotonics.5b00236
ACS Photonics 2015, 2, 1698−1704

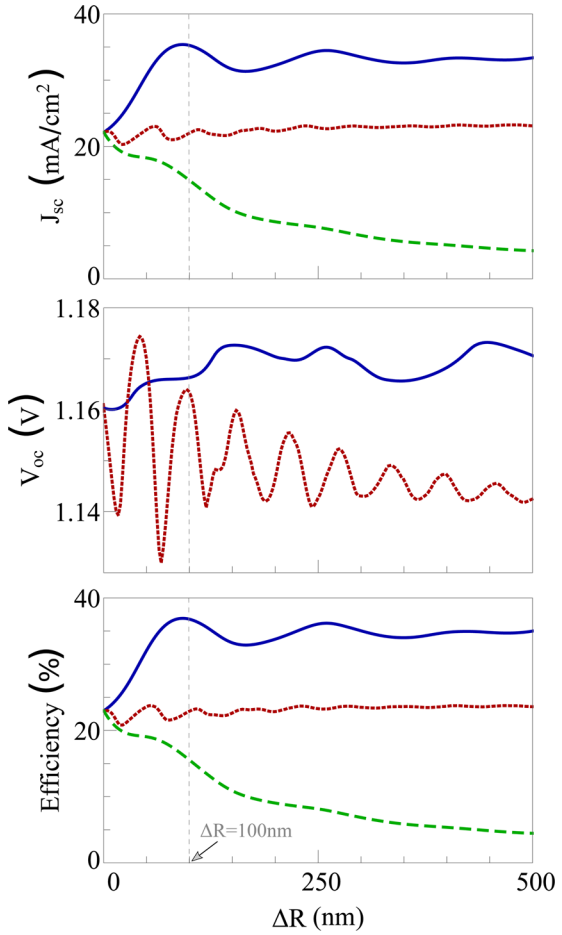

Figure 5. Solid blue lines plot the current density−voltage (J−V) characteristics of a GaAs coaxial nanowire as a function of the thickness ΔR of its outer layer Al_2O_3 coating. The GaAs section in this coaxial case has a radius r = 73 nm. Dotted red lines plot the J−V characteristics of a bare GaAs nanowire with a radius equal to the coaxial wire's total radius, i.e., 73 nm + ΔR. Characteristics shown are (a) short-circuit current density J_{sc}, (b) open-circuit voltage V_{oc} across cell, and (c) efficiency of cell at the maximum power point. The green dashed lines in parts (a) and (c) plot the current density and efficiency, respectively, calculated using the total geometrical cross-section of the coaxial wire, i.e., r = 73 nm + ΔR in eq 4. Vertical gray dashed line across all plots indicates the Al_2O_3 thickness location for the absorption efficiency plots in Figures 3 and 4

when one is primarily concerned with absorption material cost. We could also normalize J and, thus, the efficiency to the total geometrical cross-section area of the coaxial wire, i.e., using r = 73 nm + ΔR in eq 4. Such a normalization is depicted by the green lines in Figure 5, which shows the expected decrease in efficiency with an increase in ΔR, because of a reduction in the fraction of the absorber area. Although our discussions below will use the normalization to the absorber area, i.e., the blue lines in Figure 5, we note that in practice the effectiveness of any nanophotonic light-trapping scheme needs to take into account both the material and the efficiency costs.

Figure 5a shows that there is a significant enhancement in the J_{sc} of the coaxial wire over that of the bare GaAs wire for all thicknesses $\Delta R > 0$. For example, in the case of ΔR = 100 nm, i.e., vertical gray dashed line in Figure 5a, the coaxial wire's J_{sc} is enhanced by ∼60%. This strong J_{sc} enhancement is expected from the broad-band enhancement in the coaxial cell's normal incident absorption efficiency spectrum in Figure 4 (which enhances the cell's radiative generation rate F_g).

Furthermore, Figure 5b shows that the coaxial cell has a slightly enhanced V_{oc} over that of the bare GaAs wire cell with the same absorbing volume.[16] We can illustrate the physics behind this voltage enhancement using the example GaAs-Al_2O_3 coaxial wire with ΔR = 100 nm, whose normal incidence absorption spectrum is shown in Figure 4. Particularly, the V_{oc} for the GaAs-based coaxial wire is strongly influenced by the contrast ratio betwen F_g, and the thermal equilibrium radiative recombination rate F_{co} (eq 5). F_{co}, in turn, is strongly influenced by the absorption in the immediate vicinity of the band gap over all incident angles.[16] For the coaxial wire, its absorption efficiency near the band gap is slightly enhanced over that of the bare GaAs wire (one can see this for the normal incidence case in Figure 4). Therefore, the coaxial wire has a higher F_{co} as compared to the bare wire. On the other hand, the coaxial wire's net absorption efficiency enhancement for all photon energies over that of the bare wire in Figure 4 results in a large F_g enhancement. Moreover, this large F_g enhancement of the coaxial wire more than compensates its F_{co} enhancement over the bare wire. Consequently, the V_{oc} of the coaxial wire is slightly enhanced over that of the bare wire.

In addition, we see in Figure 5 some strong variations in the J−V characteristics of the coaxial wire for small Al_2O_3 thicknesses ΔR. These variations are coherent effects due to the behavior of the resonances in the absorption spectrum, as discussed in ref 16. In particular, varying ΔR changes the number of resonances in the wire that contribute to the light absorption process and also shifts the resonances in the absorption spectrum. The J_{sc} value at each thickness ΔR depends on the match between this absorption spectrum and the solar spectrum, while the V_{oc} value is strongly influenced by the presence or absence of resonances in the immediate vicinity of the electronic band gap.

The advantages of the coaxial nanowire is not restricted to the GaAs-based system. As a final example, we present the J−V characteristics of a coaxial Si wire coated with an outer layer of SiO_2. The material parameters required for calculating the absorption spectra of the Si-SiO_2 coaxial wire were extracted from ref 27. Similar to the detailed balance analysis of the GaAs-Al_2O_3 coaxial nanowire, we consider only intrinsic recombination mechanisms in our J−V calculations for the Si-SiO_2 coaxial wire. This includes only radiative and Auger recombinations. For Auger recombination, following refs 30 and 31 we assume that the Si absorbing volume is intrinsic under illumination and use the Auger coefficients given in ref 31. We also note that the detailed balance analysis of a single bare Si nanowire was recently presented in ref 15.

The blue solid lines in Figure 6 show the J−V characteristics of the Si-SiO_2 coaxial wire as a function of the thickness ΔR of its SiO_2 coating (with the absorbing Si section's radius fixed at r = 200 nm). The red dotted lines in Figure 6 plot the J−V characteristics for a bare Si nanowire with the same total radius 200 nm + ΔR as the coaxial wire. As an illustration, the green dashed lines in Figure 6a and c plot the coxial wire's current density and efficiency, respectively, calculated using its total geometrical cross-section, i.e., using r = 200 nm + ΔR in eq 4.

Similar to the GaAs-Al_2O_3 coaxial wire case in Figure 5(a), Figure 6a shows a large J_{sc} enhancement of the Si-SiO_2 coaxial wire over that of a bare Si wire with radius r = 200 nm. For example, a $\Delta R \gtrsim$ 55 nm outer SiO_2 coating gives a >50% J_{sc} enhancement over that of the bare Si wire with the same

DOI: 10.1021/acsphotonics.5b00236
ACS Photonics 2015, 2, 1698−1704

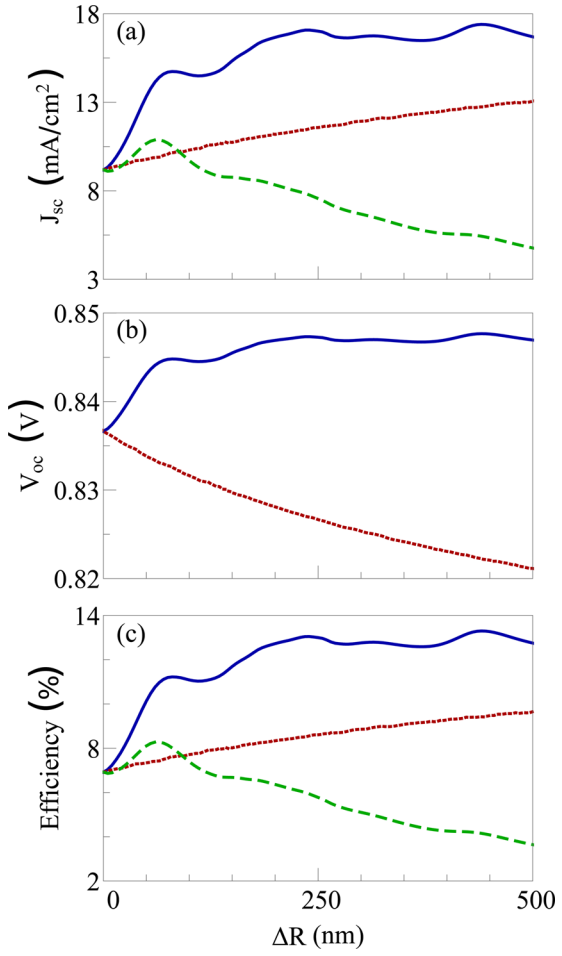

Figure 6. Solid blue lines plot the current density−voltage (J−V) characteristics of a Si coaxial nanowire as a function of the thickness ΔR of its outer layer SiO_2 coating. The Si section in this coaxial case has a radius r = 200 nm. Dotted red lines plot the J−V characteristics of a bare Si nanowire with a radius equal to the coaxial wire's total radius, i.e., 200 nm + ΔR. Characteristics shown are (a) short-circuit current density J_{sc}, (b) open-circuit voltage V_{oc} across cell, and (c) efficiency of cell at the maximum power point. The green dashed lines in parts (a) and (c) plot the current density and efficiency, respectively, calculated using the total geometrical cross-section of the coaxial wire, i.e., r = 200 nm + ΔR in eq 4.

absorbing volume. In addition, the V_{oc} of the coaxial wire is also slightly enhanced over that of the bare wire in Figure 6b.

In summary, we have shown that coating a nanowire solar cell with an oxide layer of small thickness, while keeping the nanowire's absorbing volume fixed, can significantly enhance the J−V performance of the nanowire solar cell. For example, in both GaAs-Al_2O_3 and Si-SiO_2 coaxial nanowires, we showed >50% enhancements in both J_{sc} and efficiency with an oxide layer thickness of $\Delta R \approx 65$ nm. In addition, for all oxide layer thicknesses, the coaxial wire also has a slight V_{oc} enhancement over the bare wire. One could, for example, foresee a similar J−V enhancement in a coaxial wire array, with a wire to wire spacing greater than the calculated absorption cross-section of the single coaxial nanowire discussed here. Finally, although the discussions above have focused on the optical properties of the nanowire, adding an oxide layer is also a natural surface passivation technique that can help mitigate surface recombination losses.[33,34]

AUTHOR INFORMATION

Corresponding Author

*E-mail: shanhui@stanford.edu.

Notes

The authors declare no competing financial interest.

ACKNOWLEDGMENTS

This work is supported by the Department of Energy Grant No. DE-FG07ER46426, by the Bay Area Photovoltaics Consortium (BAPVC), and by the Global Climate and Energy Project (GCEP) of Stanford University.

REFERENCES

(1) Green, M. In *Proceedings of ISES World Congress 2007 (Vol. I−Vol. V)*; Goswami, D., Zhao, Y., Eds.; Springer: Berlin Heidelberg, 2009; pp 96−101.

(2) Atwater, H. A.; Polman, A. Plasmonics for Improved Photovoltaic Devices. *Nat. Mater.* **2010**, *9*, 205−213.

(3) Picraux, S.; Yoo, J.; Campbell, I.; Dayeh, S.; Perea, D. In *Semiconductor Nanostructures for Optoelectronic Devices*; Yi, G.-C., Ed.; NanoScience and Technology; Springer: Berlin Heidelberg, 2012; pp 297−328.

(4) Beard, M. C.; Luther, J. M.; Nozik, A. J. The Promise and Challenge of Nanostructured Solar Cells. *Nat. Nanotechnol.* **2014**, *9*, 951−954.

(5) Bohren, C. F.; Huffman, D. R. *Absorption and Scattering of Light by Small Particles*, 1st ed.; Wiley Science: New York, 1983; Chapter 3, p 8.

(6) Tian, B.; Zheng, X.; Kempa, T. J.; Fang, Y.; Yu, N.; Yu, G.; Huang, J.; Lieber, C. M. Coaxial Silicon Nanowires as Solar Cells and Nanoelectronic Power Sources. *Nature* **2007**, *449*, 885−889.

(7) Cao, L.; White, J. S.; Park, J.-S.; Schuller, J. A.; Clemens, B. M.; Brongersma, M. L. Engineering Light Absorption in Semiconductor Nanowire Devices. *Nat. Mater.* **2009**, *8*, 643−647.

(8) Yan, R.; Gargas, D.; Yang, P. Nanowire Photonics. *Nat. Photonics* **2009**, *3*, 569−576.

(9) Hochbaum, A. I.; Yang, P. Semiconductor Nanowires for Energy Conversion. *Chem. Rev.* **2010**, *110*, 527−546.

(10) Garnett, E. C.; Brongersma, M. L.; Cui, Y.; McGehee, M. D. Nanowire Solar Cells. *Annu. Rev. Mater. Res.* **2011**, *41*, 269−295.

(11) Kempa, T. J.; Cahoon, J. F.; Kim, S.-K.; Day, R. W.; Bell, D. C.; Park, H.-G.; Lieber, C. M. Coaxial Multishell Nanowires with High-Quality Electronic Interfaces and Tunable Optical Cavities for Ultrathin Photovoltaics. *Proc. Natl. Acad. Sci. U. S. A.* **2012**, *109*, 1407−1412.

(12) Pan, C.; Niu, S.; Ding, Y.; Dong, L.; Yu, R.; Liu, Y.; Zhu, G.; Wang, Z. L. Enhanced Cu2S/CdS Coaxial Nanowire Solar Cells by Piezo-Phototronic Effect. *Nano Lett.* **2012**, *12*, 3302−3307.

(13) Krogstrup, P.; Jorgensen, H. I.; Heiss, M.; Demichel, O.; Holm, J. V.; Aagesen, M.; Nygard, J.; Fontcuberta i Morral, A. Single-Nanowire Solar Cells beyond the Shockley-Queisser Limit. *Natu. Photonics* **2013**, *7*, 1749−4885.

(14) Kosten, E. D.; Atwater, J. H.; Parsons, J.; Polman, A.; Atwater, H. A. Highly Efficient GaAs Solar Cells by Limiting Light Emission Angle. *Light: Sci. Appl.* **2013**, *2*, e45.

(15) Zhai, X.; Wu, S.; Shang, A.; Li, X. Limiting Efficiency Calculation of Silicon Single-Nanowire Solar Cells with Considering Auger Recombination. *Appl. Phys. Lett.* **2015**, *106*, 063904.

(16) Sandhu, S.; Yu, Z.; Fan, S. Detailed Balance Analysis and Enhancement of Open-Circuit Voltage in Single-Nanowire Solar Cells. *Nano Lett.* **2014**, *14*, 1011−1015.

(17) Mann, S. A.; Garnett, E. C. Extreme Light Absorption in Thin Semiconductor Films Wrapped around Metal Nanowires. *Nano Lett.* **2013**, *13*, 3173−3178.

(18) Oener, S. Z.; Mann, S. A.; Sciacca, B.; Sfiligoj, C.; Hoang, J.; Garnett, E. C. Au-Cu2O Core-Shell Nanowire Photovoltaics. *Appl. Phys. Lett.* **2015**, *106*, 023501.

DOI: 10.1021/acsphotonics.5b00236
ACS Photonics 2015, 2, 1698−1704

(19) Yu, Y.; Ferry, V. E.; Alivisatos, A. P.; Cao, L. Dielectric CoreShell Optical Antennas for Strong Solar Absorption Enhancement. *Nano Lett.* **2012**, *12*, 3674−3681.
(20) Yu, Y.; Huang, L.; Cao, L. Semiconductor Solar Superabsorbers. *Sci. Rep.* **2014**, *4*, 04107.
(21) Miller, O. D.; Yablonovitch, E.; Kurtz, S. R. Strong Internal and External Luminescence as Solar Cells Approach the Shockley-Queisser Limit. *IEEE J. Photovolt.* **2012**, *2*, 303−311.
(22) Yu, Z.; Raman, A.; Fan, S. Fundamental Limit of Nanophotonic Light Trapping in Solar Cells. *Proc. Natl. Acad. Sci. U. S. A.* **2010**, *107*, 17491−17496.
(23) Jacob, Z.; Alekseyev, L. V.; Narimanov, E. Optical Hyperlens: Far-Field Imaging beyond the Diffraction Limit. *Opt. Express* **2006**, *14*, 8247−8256.
(24) Ruan, Z.; Fan, S. Superscattering of Light from Subwavelength Nanostructures. *Phys. Rev. Lett.* **2010**, *105*, 013901.
(25) Wait, J. R. Scattering of a Plane Wave from a Circular Dielectric Cylinder at Oblique Incidence. *Can. J. Phys.* **1955**, *33*, 189−195.
(26) Abramowitz, M.; Stegun, I. A. *Handbook of Mathematical Functions: with Formulas, Graphs, and Mathematical Tables*; 1972; http://people.maths.ox.ac.uk/~macdonald/aands/page_360.htm.
(27) Palik, E. D. *Handbook of Optical Constants of Solids: Vol. 1*; Elsevier Academic Press: Waltham, MA, 1985; pp 429, 547, 749.
(28) Palik, E. D. *Handbook of Optical Constants of Solids: Vol. 2*; Elsevier Academic Press: Waltham, MA, 1985; p 761.
(29) Shockley, W.; Queisser, H. J. Detailed Balance Limit of Efficiency of p-n Junction Solar Cells. *J. Appl. Phys.* **1961**, *32*, 510−519.
(30) Green, M. Limits on the Open-Circuit Voltage and Efficiency of Silicon Solar Cells Imposed by Intrinsic Auger Processes. *IEEE Trans. Electron Devices* **1984**, *31*, 671−678.
(31) Tiedje, T.; Yablonovitch, E.; Cody, G. D.; Brooks, B. G. Limiting Efficiency of Silicon Solar Cells. *IEEE Trans. Electron Devices* **1984**, *31*, 711−716.
(32) Kayes, B.; Nie, H.; Twist, R.; Spruytte, S.; Reinhardt, F.; Kizilyalli, I.; Higashi, G. 27.6% Conversion Efficiency, a New Record for Single-Junction Solar Cells under 1 Sun Illumination. *37th IEEE Photovoltaic Specialists Conference (PVSC)* **2011**, 000004−000008.
(33) Dingemans, G.; van de Sanden, M. C. M.; Kessels, W. M. M. Excellent Si Surface Passivation by Low Temperature SiO2 Using an Ultrathin Al2O3 Capping Film. *Phys. Status Solidi RRL* **2011**, *5*, 22−24.
(34) Mariani, G.; Scofield, A. C.; Hung, C.-H.; Huffaker, D. L. GaAs Nanopillar-Array Solar Cells Employing In-Situ Surface Passivation. *Nat. Commun.* **2013**, *4*, 1497.

DOI: 10.1021/acsphotonics.5b00236
ACS Photonics 2015, 2, 1698−1704